Structure of Protonated Carbon Dioxide Clusters: Infrared Photodissociation Spectroscopy and ab Initio Calculations

G. E. Douberly, A. M. Ricks, B. W. Ticknor, and M. A. Duncan*

Department of Chemistry, University of Georgia, Athens, Georgia 30602-2556

Received: October 9, 2007; In Final Form: November 5, 2007

The infrared photodissociation spectra (IRPD) in the 700 to 4000 cm^{-1} region are reported for $H^+(CO_2)_n$ clusters ($n = 1-4$) and their complexes with argon. Weakly bound Ar atoms are attached to each complex upon cluster formation in a pulsed electric discharge/supersonic expansion cluster source. An expanded IRPD spectrum of the $H^+(CO_2)$Ar complex, previously reported in the 2600−3000 cm^{-1} range [Dopfer, O.; Olkhov, R.V.; Roth, D.; Maier, J.P. *Chem. Phys. Lett.* **1998**, *296*, 585−591] reveals new vibrational resonances. For $n = 2$ to 4, the vibrational resonances involving the motion of the proton are observed in the 750 to 1500 cm^{-1} region of the spectrum, and by comparison to the predictions of theory, the structure of the small clusters are revealed. The monomer species has a nonlinear structure, with the proton binding to the lone pair of an oxygen. In the dimer, this nonlinear configuration is preserved, with the two CO_2 units in a trans configuration about the central proton. Upon formation of the trimer, the core CO_2 dimer ion undergoes a rearrangement, producing a structure with near C_{2v} symmetry, which is preserved upon successive CO_2 solvation. While the higher frequency asymmetric CO_2 stretch vibrations are unaffected by the presence of the weakly attached Ar atom, the dynamics of the shared proton motions are substantially altered, largely due to the reduction in symmetry of each complex. For $n = 2$ to 4, the perturbation due to Ar leads to blue shifts of proton stretching vibrations that involve motion of the proton mostly parallel to the $O-H^+-O$ axis of the core ion. Moreover, proton stretching motions perpendicular to this axis exhibit smaller shifts, largely to the red. Ab initio (MP2) calculations of the structures, complexation energies, and harmonic vibrational frequencies are also presented, which support the assignments of the experimental spectra.

Introduction

The structural characterization of the accommodation of protons on molecular frameworks is central to developing a microscopic understanding of biological processes such as proton transport across membranes,[1−3] enzymic catalysis,[4,5] and proton transfer in acidic, aqueous environments.[6−8] Common to many of these systems are strong ionic hydrogen-bonding motifs of the form $O\cdots H^+\cdots O$.[9] Characterization of the broad, low barrier proton-transfer potentials involved in these systems is essential for a quantitative description of the microscopic phenomena. Theoretical and experimental cluster studies of the structural and dynamical properties of the solvated proton have been a topic of ongoing interest for the last several years. Recent progress in this direction includes size-specific, infrared spectroscopic,[10−13] and theoretical[13b, 14−16] studies of the evolution of the proton accommodation motif in small water clusters, providing insight into the high mobility of the proton in acidic, aqueous media.[7] Indeed, a sensitive probe of the structure of the shared proton bond is the infrared spectral signature of the shared proton motion. Both homogeneous and heterogeneous gas-phase protonated dimers of the form $R'O\cdots H^+\cdots OR$ have been investigated with infrared multiphoton dissociation (IRMPD) spectroscopy employing high power, free-electron lasers that are capable of probing the vibrational resonances involving the shared proton (ν_{sp}).[17,18] More recently, Roscioli et al. have extended these studies,[19] using a lower power OPO/OPA infrared system and the method of rare gas tagging[20−24] to probe ν_{sp} with higher resolution and for a broader class of mixed dimers. In the present study, we employ infrared photodissociation spectroscopy (IRPD) along with rare gas tagging to probe the vibrational resonances associated with the shared proton motions in small protonated carbon dioxide clusters. Carbon dioxide provides a prototype for the interaction of the proton with sp^2-hybridized oxygen atoms within carbonyl groups. The IRPD spectra in the 750−1500 cm^{-1} range provide insight into the effect of the local solvation environment on the $O\cdots H^+\cdots O$ bonding motif and the proton-transfer potential in these clusters.

The assignment of interstellar millimeter wave bands to protonated CO_2, $(OCOH)^+$,[25] motivated several laboratory,[26−30] and theoretical ab initio[31−34] studies of the ion. The pure rotational spectrum in the sub-millimeter wavelength region,[29,30] along with high-resolution ro-vibrational absorption spectroscopy of the fundamental ν_1 OH^+ stretch,[27,28] confirmed the original assignment. More recently, the FTIR spectrum of $(OCOH)^+$ has been measured in solid neon,[35] and the complexes of $(OCOH)^+$ with Ar, Ne, and He were measured with IRPD in the 3 μm region,[36] revealing a progressively larger red shift of the OH^+ stretch with increasing polarizability of the rare gas atom. For the $H^+(CO_2)_n$ clusters ($n > 1$), bond enthalpies have been measured with high-pressure mass spectrometry,[37,38] and the results are in good agreement with the incremental CO_2 binding energies obtained from ab initio calculations.[38,39] However, there is no previous spectroscopy of the larger clusters. With the broadly tunable infrared laser systems now available, we are able to probe the region of the shared proton motion in the larger clusters. By comparison with the predictions from

* Author to whom correspondence should be addressed. E-mail: maduncan@uga.edu.

10.1021/jp7098587 CCC: $40.75 © 2008 American Chemical Society
Published on Web 01/15/2008

theory, the structure of the larger $H^+(CO_2)_n$ ($n = 2-4$) clusters and the sites of proton binding are revealed.

Experimental Methods

Protonated CO_2 and its clusters are produced in a pulsed high voltage electric discharge source coupled to a pulsed nozzle supersonic expansion. Two 1 mm diameter sewing needles are mounted in a Teflon block on the faceplate of a 0.5 mm diameter General Valve (series 9). The needle tips are separated by approximately 0.5 mm and are centered on the beam axis 5 mm downstream from the valve orifice. An approximately 1 μs wide, -1200 V pulse is generated with a DEI Model PVX-4140 high voltage pulser. With one needle grounded, the high voltage pulse is applied to the other needle, which produces a discharge in the center of the 250−300 μs wide gas pulse. Collisional cooling in the expansion leads to cations with estimated temperatures below 50 K.[40] The gas mixture consists of 0.5% CO_2, 10% H_2, 10% Ar, and a balance consisting of a 70%/30% mixture of Ne and He. The expansion is collimated 15 cm downstream by a 2 mm diameter conical skimmer and passes into a second differentially pumped chamber.

Cations produced in the discharge are pulse extracted into a reflectron time-of-flight mass spectrometer, which is mounted perpendicular to the molecular beam axis. Mass selection of a specific ion is achieved with pulsed deflection plates located in the first of two flight tube sections. Resonant IRPD occurs in the turning region of the reflectron field by overlapping the ion packet with the tunable output of an infrared OPO/OPA laser system (LaserVision). The OPO, consisting of a single potassium titanyl phosphate (KTP) crystal, is pumped by a 10 Hz, injection-seeded Nd:YAG laser (Spectra Physics model PRO-230, equipped with "BeamLok"). The 2000−4000 cm^{-1} frequency range is obtained by mixing the tunable 1.5 μm OPO idler beam with the Nd:YAG fundamental in four potassium titanyl arsenate (KTA) crystals, producing a tunable 2.5−5.0 μm beam with typical pulse energies between 1 and 10 mJ. The lower energy 700−2000 cm^{-1} region is obtained by mixing the 1.5 and 3.0 μm beams in a $AgGaSe_2$ crystal, producing approximately 300 μJ/pulse at 900 cm^{-1}. The bandwidth of the OPO/OPA system is ~1.5 cm^{-1}, and the infrared wavelength is calibrated with optoacoustic spectra of CH_4 in an external gas cell.

Fragments resulting from resonant photodissociation are separated from any residual parent ions by their flight time in the second flight tube of the mass spectrometer. As the infrared wavelength is tuned, mass specific infrared spectra are recorded by monitoring the fragment ion signal with a digital oscilloscope (LeCroy WaveRunner 6051A). The fragment signal is normalized to the parent ion signal to correct for long-term fluctuations in the ion source.

Theoretical Methods. Ab initio calculations are carried out at the MP2(fc) level of theory for the $H^+(CO_2)_n$ and $H^+(CO_2)_n$–Ar complexes with a split valence 6-311++G(2d,2p) basis set employing the GAMESS program package.[41] The results from harmonic frequency calculations are scaled by a factor of 0.96 for comparison to the IRPD spectra.[42] Reported binding energies of Ar to the protonated CO_2 clusters are counterpoise corrected[43] throughout. Full details of the ab initio calculations for each cluster size are provided in the Supporting Information, including structures, energetics, and detailed assignments of the vibrational harmonic frequencies.

Results and Discussion

The mass spectrum of ions produced in the pulsed electric discharge source is shown in Figure 1. The gas mixture is 10% H_2, resulting in the exclusive formation of $H^+(CO_2)_n$ clusters as opposed to the unprotonated $(CO_2)^+_n$ species.[44] Cluster sizes up to approximately $n = 60$ are produced, and the peak in the ion distribution can be modified by adjusting the relative timing of the gas and high voltage pulses. Moreover, there are no apparent cluster sizes which appear intrinsically stable, such as the $n = 21$ protonated water cluster.[45] The larger $H^+(CO_2)_n$ clusters ($n \geq 5$) have external CO_2 subunits that are bound to the cluster by less than 1000 cm^{-1}, and the IRPD spectra can be obtained in the loss of CO_2 channel. However, the increase in binding energy of CO_2 in the $n < 5$ clusters preclude the fragmentation of the cluster with single photon absorption, and the rare gas tagging method[20−24] is required to obtain the IRPD spectra in the 700−4000 cm^{-1} range. For example, from the ab initio calculations, the most weakly bound CO_2 subunit has a binding energy of 12700, 3080, and 2960 cm^{-1}, for the $n = 2$, 3, 4 clusters, respectively. In comparison, Ar is bound by only ~600 cm^{-1} to all cluster sizes. Upon addition of Ar to the expansion gas mixture (~10%), efficient clustering of Ar with the $H^+(CO_2)_n$ clusters is observed. Figure 2 shows the resulting mass spectrum of the ions produced, with as many as 6 Ar atoms attached to the $n = 1$ to 4 clusters.

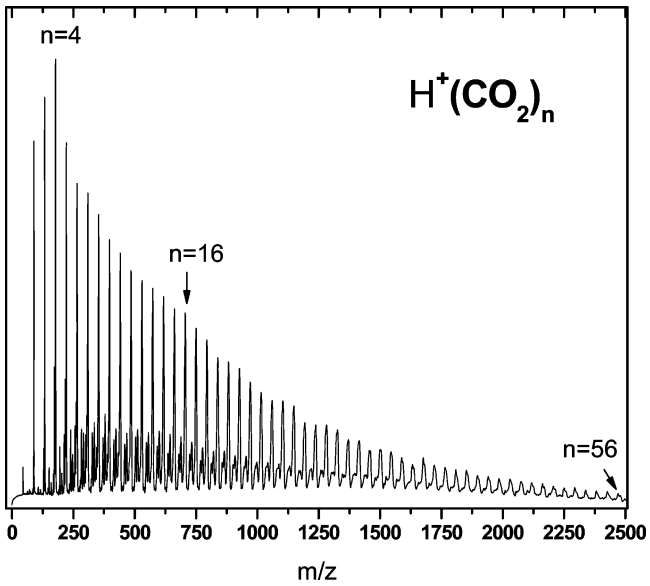

Figure 1. Mass spectrum of the ions produced in the pulsed electric discharge cluster ion source. The expansion mixture consists of CO_2, H_2, Ne, and He present in a 1:25:40:90 ratio. $H^+(CO_2)_n$ clusters are produced for sizes up to approximately $n = 60$.

$H^+(CO_2)$−Ar. Previous ab initio calculations[31−34,46,47] on $(OCOH)^+$ have predicted a trans bent structure with the protonation occurring on the oxygen lone pair, whose bonding loses the sp^2 character associated with neutral, linear CO_2. Ground state rotational constants obtained from the sub-millimeter wave spectra[29] are consistent with the trans bent structure predicted by theory. Amano and co-workers have measured the ν_1 fundamental (OH stretch) of $(OCOH)^+$ with direct absorption techniques, and the vibrational band origin is located at 3375.374 cm^{-1}.[27] More recently, Dopfer and co-workers reported ab initio calculations and the IRPD spectrum of $(OCOH)^+$Ar in the 2600−3000 cm^{-1} region.[36] The ab initio MP2 calculations, reproduced here, find that the Ar is bound on the proton. As a result of complexation, the OH bond is lengthened by 0.03 Å, and the HOC bond angle increases by 2°. The calculated binding energy of the Ar to $(OCOH)^+$ in the ground vibrational state is approximately 2400 cm^{-1}.

In the complex, the proton becomes somewhat shared between CO_2 and Ar, although asymmetrically. The OH^+ and H^+Ar bond

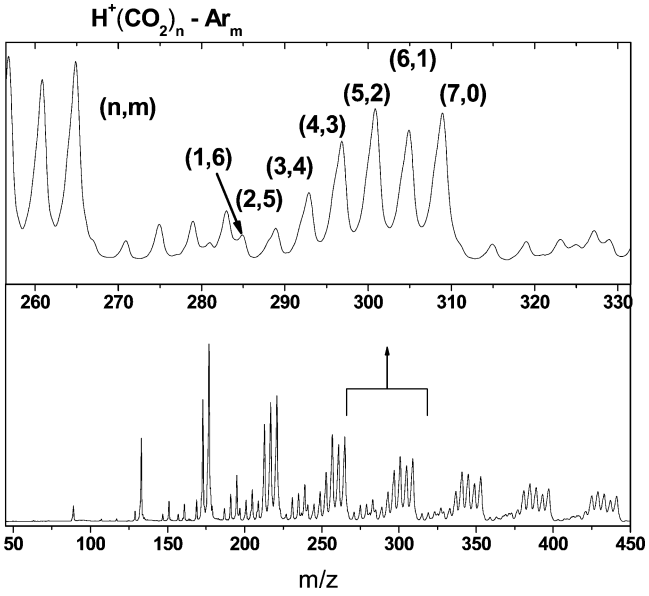

Figure 2. Mass spectrum of $H^+(CO_2)_nAr_m$ clusters produced upon addition of Ar to the expansion mixture. As shown in the inset, complexation of Ar with $H^+(CO_2)_n$ is efficient, with up to $m = 6$ being produced for values of $n < 7$.

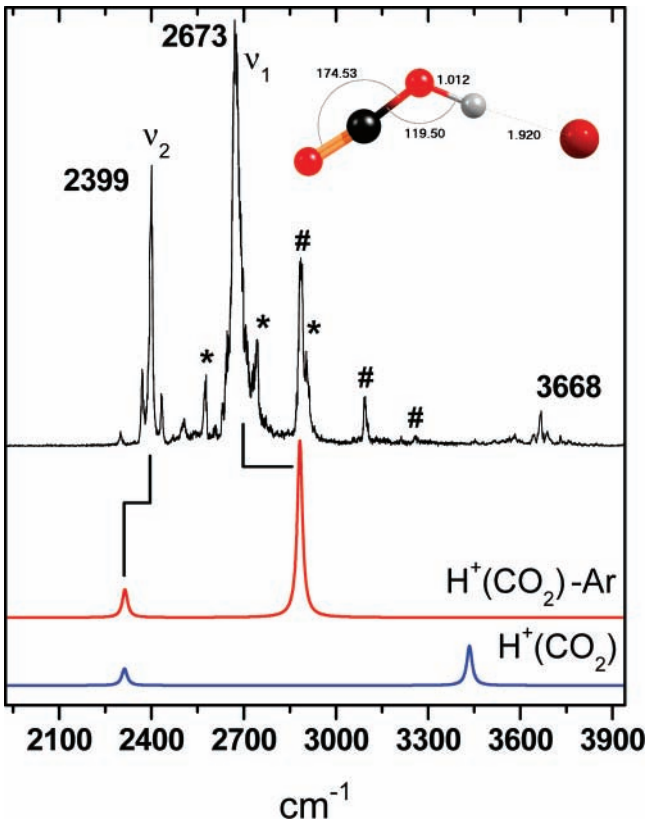

Figure 3. IRPD spectrum of $H^+(CO_2)Ar$ measured in the Ar loss channel. The bands marked by # and ∗ are assigned to H^+-Ar stretch progressions in the excited v_1 and v_2 vibrational states, respectively. The ab initio MP2(fc) 6-311++g(2d,2p) spectra for the $H^+(CO_2)Ar$ (red) and $H^+(CO_2)$ (blue) complexes are shown for comparison. Both theoretical spectra are presented with correct relative IR intensities.

lengths are 1.012 and 1.920 Å, respectively, as shown in the inset of Figure 3. The Ar-induced geometry change of $(OCOH)^+$ results in a significant (704 cm^{-1}) red shift of the OH stretch. The IRPD spectra of the OH stretch region in $(OCOH)^+$-Rg (Rg = He, Ne, Ar)[36] revealed a linear dependence of the experimental red shift with the proton affinity (PA) of the rare gas atom. Indeed, with regards to a one-dimensional representation of the proton-transfer coordinate, the shared proton potential becomes more asymmetric and broader as the PA of the rare gas atom approaches the PA of CO_2 (540.2 kJ/mol).[48] This effect has been observed and discussed by Johnson and co-workers, who studied the shared proton stretch vibrational band origins of various $R'-O\cdots H^+\cdots O-R$ species.[19] As a general trend, the frequency of the shared proton motions increased as the difference in PA, ΔPA, of the two subunits increased.

The IRPD spectrum of $(OCOH)^+Ar$ is shown in Figure 3 along with the predicted spectra from the MP2 harmonic frequency calculations. The experimental and ab initio frequencies along with the assignments are summarized in Table 1. We have extended the range previously recorded by Dopfer[36] to include the entire 1000−4000 cm^{-1} region of the mid-IR, revealing many additional bands. Given the ab initio binding energy of Ar (∼2400 cm^{-1}), photodissociation leading to the loss of Ar is not expected to be efficient below this photon energy. As a result, no vibrational bands are observed below ∼2300 cm^{-1}, which includes the region of the ν_3 OCO symmetric stretch. Once again, a large (552 cm^{-1}) complexation induced red shift of the OH stretch is predicted by the harmonic frequency calculations. Additionally, an intensity enhancement is predicted, originating from the increased dipole induced polarization of Ar in the excited vibrational state. The IRPD spectrum in the 2600−3000 cm^{-1} range is in excellent agreement with the spectrum reported previously.[36] The most intense feature centered at 2673 cm^{-1} is again assigned to the (shared proton, ν_{sp}) OH^+ stretch, corresponding to a red shift from $(OCOH)^+$ of 702(3) cm^{-1}.[27] The red shift observed for the complex is 150 cm^{-1} greater than the prediction from theory, demonstrating the inability of the harmonic approximation to adequately describe the anharmonic shared proton stretching motion.[13b] The second most intense feature, centered at 2399 cm^{-1}, is assigned to the asymmetric OCO stretching vibration (ν_2), corresponding to a 50 cm^{-1} blue shift from the band origin of the analogous vibration in neutral, linear CO_2. Unfortunately, we are unable to compare the ν_2 band origin of $(OCOH)^+Ar$ to that of isolated $(OCOH)^+$. Nevertheless, although the ab initio calculations show an enhanced intensity for the ν_2 stretch, a negligible frequency shift (<1 cm^{-1}) from isolated $(OCOH)^+$ is predicted.

While the harmonic frequency calculations predict only two bands, there are many weaker features spanning the entire 2300 to 3800 cm^{-1} region. The band centered at 2884 cm^{-1} was also observed by Dopfer[36] and assigned to the $\nu_1+\nu_s$ combination band, where ν_s corresponds to the $(OCOH^+)-Ar$ stretch (211 cm^{-1}), which is in reasonable agreement with the ab initio value (184 cm^{-1}). In addition to the 2884 cm^{-1} band, we find two additional bands at 3093 and 3256 cm^{-1}, which are indicated (#) in Figure 3. Given the frequency spacing between the 2673, 2884, 3093, and 3256 cm^{-1} bands, we assign this as a progression of the $\nu_1+n\nu_s$ combination bands ($n = 0-3$), corresponding to the simultaneous vibrational excitation of the OH^+ stretch and the fundamental/overtones of the $(OCOH^+)-Ar$ stretch. Closer inspection of the region to the blue of the ν_2 fundamental reveals another regular progression of bands, which are also indicated (∗) in Figure 3. The bands centered at 2399, 2575, 2744, and 2905 cm^{-1} are similarly assigned to a $\nu_2+n\nu_s$ progression ($n = 0-3$), with the last two bands appearing on the shoulders of the 2673 and 2884 cm^{-1} bands.

Treating $(OCOH)^+$ and Ar as a pseudodiatomic, we can estimate the $(OCOH^+)-Ar$ stretching frequency and the complex dissociation energy in both the ν_1 and ν_2 excited states.

TABLE 1: A Selection of MP2(fc) 6-311++g(2d,2p) ab Initio Vibrational Frequencies and Intensities for $H^+(CO_2)_n$ (n = 1, 2) and Their Complexes with Ar

isomer	ab initio[a] cm^{-1} (km/mol)	experimental (cm^{-1})	assignment[b]
$H^+(CO_2)$	3434.48 (633)	3375.37[c]	OH str.
	2312.12 (269)		OCO asym. str.
$H^+(CO_2)Ar$	2882.69 (2770)	2673(3)	OH str.
	2313.53 (438)	2399(2)	OCO asym. str.
	184.17 (51)	183,[d] 243[e]	$(OCOH)^+$Ar str.
$H^+(CO_2)_2$	2331.19 (8)		ooph OCO asym. str.
	2327.07 (670)		iph OCO asym. str.
	1336.59 (570)		ip $\nu_{sp}(\perp)$
	1281.23 (1)		iph OCO sym. str.
	1230.19 (40)		ooph OCO sym. str.
	982.04 (104)		oop $\nu_{sp}(\perp)$
	762.72 (5300)		ip $\nu_{sp}(\parallel)$
$H^+(CO_2)_2Ar$	2331.97 (203)	2400	ooph OCO asym. str.
	2327.50 (407)	2400	iph OCO asym. str.
	1385.68 (1800)	1345, 1445	ip $\nu_{sp}(\perp)$
	1279.64 (12)		iph OCO sym. str.
	1226.39 (33)		ooph OCO sym. str.
	994.34 (5300)	1026	ip $\nu_{sp}(\parallel)$
	953.27 (502)	888	oop $\nu_{sp}(\perp)$

[a] Ab initio frequencies are scaled by a factor of 0.96. [b] Notation: ip (in-plane), oop (out-of-plane), iph (in-phase), ooph (out-of-phase), ν_{sp} (shared proton motion) [c] Reference 27 [d] ω_e in the excited υ_2 vibrational state. [e] ω_e in the excited υ_1 vibrational state.

TABLE 2: Constants from a Linear Least-Squares Fit of the $(OCOH)^+$Ar Stretch Progressions of $(OCOH)^+$Ar to the Energy Level Expression of a Morse Oscillator (units are cm^{-1})

vibration	ω_e	$\omega_e x_e$	D_e	D_o
ν_1	242.2	11.8	1253	1134
ν_2	182.4	3.6	2301	2211
ab initio[a]	184		2400	

[a] MP2(fc) 6-311++g(2d,2p).

Fitting each progression to a Morse oscillator energy level expression leads to the constants in Table 2, which can be compared to the ground vibrational state ab initio values of ω_e = 184 cm^{-1} and D_e = 2400 cm^{-1}. In the excited ν_1 state, this simple pseudo-diatomic treatment gives a larger stretching frequency (243 cm^{-1}) and decreased Ar binding energy (1253 cm^{-1}) in comparison to the ab initio ground state calculations. In comparison, the excited ν_2 state values are in excellent agreement with the values predicted for the ground state equilibrium structure. Apparently, vibrational excitation of the OCO asymmetric stretch has only a minor effect on the $(OCOH)^+$−Ar intermolecular potential. If we assume that the Morse potential is a valid representation of the intermolecular potential for both excited states, then the fitted values imply that the ν_1 excited-state potential is both stiffer and more anharmonic, in comparison to ν_2. As a result of the larger anharmonicity, the intermolecular bond energy in the ν_1 excited-state is reduced. Nevertheless, given the strong coupling between the OH^+ stretch and the intermolecular $(OCOH)^+$−Ar stretch, this simple model may be insufficient with respect to the ν_1 excitation.

Other, weaker bands are observed in the lower energy region of the spectrum at 2300, 2370, 2430, 2500, and 2600 cm^{-1}. Given the binding energy of Ar in the complex, we are unable to observe vibrational bands below ~2300 cm^{-1}. The unassigned weaker features may be due to other combination bands associated with the COH^+ bending overtone. There are also weaker bands in the 3600−3800 cm^{-1} range, with the most intense band in this range located at 3668 cm^{-1}. The assignment of this band to the combination (ν_2+ν_3) of the asymmetric OCO stretch with the symmetric OCO stretch seems reasonable. Given the proximity of these features to the $(02^01)/(10^01)$ Fermi resonance in neutral CO_2,[49] the weaker features in this region may originate from combinations of ν_2 with bands in the 1240−1290 cm^{-1} region consisting of the symmetric OCO stretch in resonance with the OCO out-of-plane bend overtone, which are predicted by theory to be near 1200 and 600 cm^{-1}, respectively.

$H^+(CO_2)_2$−Ar. There have been two previous reports of ab initio calculations for the protonated CO_2 dimer.[38,39] According to these, the dimer has a "chair" structure with near C_i symmetry and a linear OH^+O bonding motif. Our calculations here at the MP2/6-311++g(2d,2p) level of theory produce the same structure, as shown in Figure 4a. These higher level calculations confirm the structure reported previously for the dimer. The proton is nearly equally shared with an OH^+O bond angle of 179.9 degrees and OH^+ bond lengths of 1.206 and 1.179 Å. In comparison to the $(OCOH)^+$Ar complex, the equilibrium OH^+ bond length has increased by ~0.18 Å, indicative of the more symmetric proton-transfer potential and equal proton sharing involved. We have investigated the proton-transfer coordinate with fully relaxed MP2 potential energy scans, which indicate that there is only a small barrier (<10 cm^{-1}) between two minima in a broad, double-well potential. Certainly, the zero-point motion of the complex leads to a vibrationally averaged structure with C_i symmetry and a proton equally shared between the two slightly bent CO_2 units.

We begin the discussion of the spectroscopy of the protonated dimer by considering in detail the ab initio harmonic frequency calculations to investigate the locations of the vibrational bands characteristic of the proton motion. The calculated spectrum of the protonated dimer is shown at the bottom of Figure 5 (blue). There are three bands predicted at 763, 982, and 1337 cm^{-1}, all of which involve the motion of the proton. The band at 763 cm^{-1} corresponds to the exchange of the proton between the oxygen lone pairs of the CO_2 subunits. The displacement vector for this normal mode is largely parallel to the ground state equilibrium OH^+O bond, and we will use the notation, $\nu_{sp}(\parallel)$, to indicate shared proton motions of this type.[19] The transition dipole moment for $\nu_{sp}(\parallel)$ is large with a calculated intensity of 5300 km/mol. We note here that the calculations predict a 2100 cm^{-1} red shift in the proton stretch frequency upon going from $OCOH^+$−Ar (ΔPA = 171 kJ/mol) to OCO−H^+−OCO (ΔPA = 0 kJ/mol), indicative of the symmetric sharing of the proton in the latter. The bands predicted at 982 and 1337 cm^{-1} are associated with the out-of-plane and in-plane proton motions,

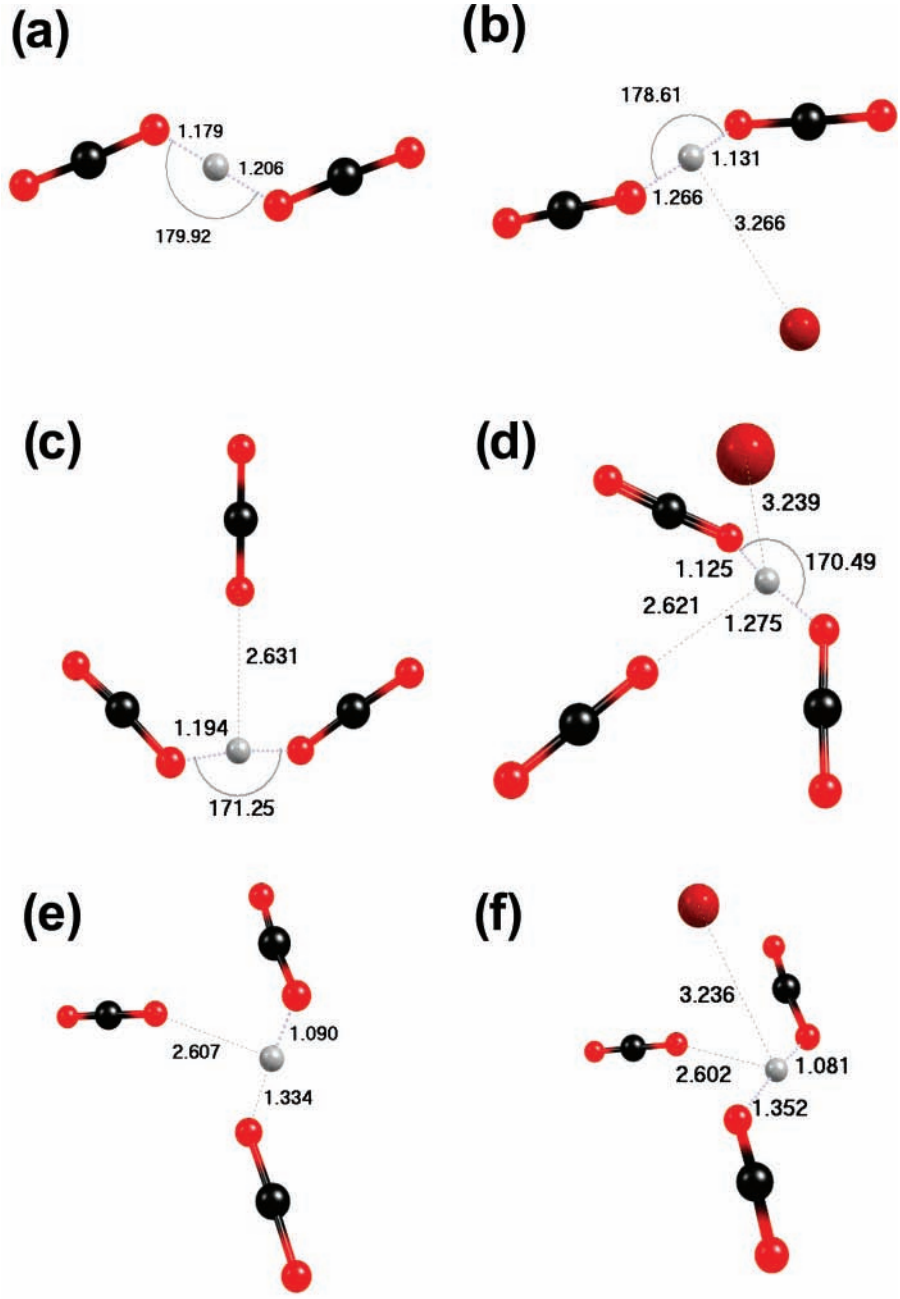

Figure 4. Ab initio structures of the $H^+(CO_2)_n$ ($n = 2, 3$) species with and without the complexation of Ar. The essentially C_i core symmetry of the (a) protonated dimer and the (c) protonated "boat" trimer is reduced to C_1 upon addition of Ar (b and d), as indicated by the O−H and O−H−O bond distances (Å) and angles (deg). Structures f and e correspond to the protonated "chair" trimer species with and without Ar, respectively.

respectively, which are largely perpendicular ($\nu_{sp}(\perp)$) to the ground state equilibrium OH^+O bond. The calculated band origins and corresponding assignments are summarized in Table 3 for the shared proton vibrations of the protonated dimer. As discussed above, previous mass selective experiments using free electron lasers[10,11,17,18] and lower power OPO laser systems[13,19] have also shown that other protonated homodimers also have shared proton motions in this region, which can be described as either parallel or perpendicular to the OH^+O bond axis.

Because the calculated energy required to fragment $H^+(CO_2)_2$ is ~36 kcal/mol (12700 cm^{-1}), we are unable to photodissociate the complex with single photon absorption. Therefore, we must apply the rare gas tagging technique to acquire the spectrum of the dimer. The calculated binding energy of Ar to the protonated dimer is 660 cm^{-1}, and Ar is therefore a favorable leaving group for the IR photodissociation technique. The structure of the $H^+(CO_2)_2$ Ar complex is shown in Figure 4b, indicating that the Ar is bound to the complex out of the plane and nominally on top of the proton with an H^+Ar bond length of 3.27 Å. With the proton enclosed between the two CO_2 units, and because 3.27 Å is significantly larger than the H^+Ar bond length in $(OCOH)^+Ar$, we initially anticipated that the Ar would not significantly perturb the vibrational dynamics of the bare protonated dimer. Nevertheless, the ab initio calculations predict that addition of Ar to the complex reduces the symmetry in the proton-transfer coordinate, leading to an asymmetric sharing of the proton and equilibrium OH^+ bond lengths of 1.131 and 1.266 Å. The calculated spectrum for the $H^+(CO_2)_2$ Ar complex is shown as the smooth red curve in Figure 5. While the in-phase and out-of-phase asymmetric CO_2 motions are unperturbed, the most noticeable effect of the Ar is to blue shift the $\nu_{sp}(\parallel)$ transition by 230 cm^{-1}. Although it is weakly bound, the presence of the Ar leads to a relatively large change in the proton stretch frequency, even for the harmonic calculation. Once again,

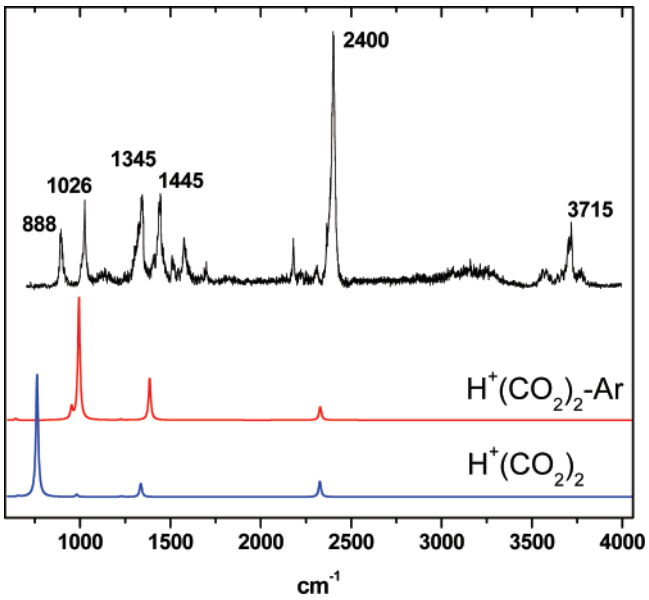

Figure 5. IRPD spectrum of $H^+(CO_2)_2Ar$ measured in the Ar loss channel. The MP2(fc) 6-311++g(2d,2p) $H^+(CO_2)_2Ar$ (red) and $H^+(CO_2)_2$ (blue) spectra are shown for comparison. Both theoretical spectra are presented with correct relative IR intensities. The most intense feature in the $H^+(CO_2)_2$ calculated spectrum, $\nu_{sp}(\parallel)$, is blue-shifted by 230 cm^{-1} upon addition of Ar to the complex.

TABLE 3: Shared Proton MP2(fc) 6-311++g(2d,2p) ab Initio Vibrational Frequencies and Intensities for the $H^+(CO_2)_n$ (n = 3, 4) and Their Complexes with Ar

isomer	ab initio[a] cm^{-1} (km/mol)	experimental (cm^{-1})	assignment[b]
$H^+(CO_2)_3$ "chair"	1682.65 (5140)		ip $\nu_{sp}(\parallel)$
	1224.52 (26)		ip $\nu_{sp}(\parallel)$
	1106.60 (2260)		ip $\nu_{sp}(\perp)$
	921.39 (243)		oop $\nu_{sp}(\perp)$
$H^+(CO_2)_3Ar$ "chair"	1781.54 (5300)		ip $\nu_{sp}(\parallel)$
	1224.08 (22)		ip $\nu_{sp}(\parallel)$
	1118.23 (1780)		ip $\nu_{sp}(\perp)$
	903.31 (164)		oop $\nu_{sp}(\perp)$
$H^+(CO_2)_3$ "boat"	1161.19 (226)		ip $\nu_{sp}(\perp)$
	1105.06 (582)		oop $\nu_{sp}(\perp)$
	803.16 (4560)		ip $\nu_{sp}(\parallel)$
	403.40 (2680)		ip $\nu_{sp}(\parallel)$
$H^+(CO_2)_3Ar$ "boat"	1356.73 (1700)	1467	ip $\nu_{sp}(\parallel)$
	1206.44 (870)	1255	ip $\nu_{sp}(\parallel,\perp)$
	1093.43 (2566)	1088	ip $\nu_{sp}(\perp)$
	976.97 (1474)	904	oop $\nu_{sp}(\perp)$
$H^+(CO_2)_4$ "boat"	1236.94 (149)		ip $\nu_{sp}(\perp)$
	973.05 (129)		oop $\nu_{sp}(\perp)$
	847.63 (4590)		ip $\nu_{sp}(\parallel)$
	376.96 (2070)		ip $\nu_{sp}(\parallel)$

[a] Ab initio frequencies are scaled by a factor of 0.96. [b] Notation: ip (in-plane), oop (out-of-plane), ν_{sp} (shared proton motion)

in agreement with previous results,[13b,19] we find that the frequency of the proton stretch vibrations in $H^+(CO_2)_2$ are extremely sensitive to subtle changes to the shape of the proton-transfer potential. As mentioned above, Johnson and co-workers have demonstrated[19] that as the difference in PA of heterodimer partners having OH^+O bonds increases, a systematic blue shift is observed for the $\nu_{sp}(\parallel)$ transition as the proton becomes more unevenly shared. For the protonated CO_2 dimer, the calculated blue shift is consistent with the Ar induced asymmetry in the proton-transfer coordinate. Upon investigation of the $\nu_{sp}(\parallel)$ normal mode coordinate, we also find that in the bare dimer, the proton stretch is accompanied by the in-phase bending/symmetric stretching motion of the CO_2 subunits. With the addition of Ar, these motions are damped for the $\nu_{sp}(\parallel)$ normal mode, leading to a more confined proton, which is also consistent with the observed blue shift.

The Ar perturbation of the two $\nu_{sp}(\perp)$ stretches is predicted to be less extensive than for $\nu_{sp}(\parallel)$. Nevertheless, a blue shift of $\sim$50 cm^{-1} is predicted for the in-plane $\nu_{sp}(\perp)$, while a 30 cm^{-1} redshift is predicted for the $\nu_{sp}(\perp)$ vibration involving the proton oscillation out of the core ion plane and into the Ar. Additionally, the presence of Ar enhances the oscillator strength of each $\nu_{sp}(\perp)$ vibration. Overall, the harmonic frequency calculations predict a rather simple spectrum with four intense vibrations in the 700 to 4000 cm^{-1} range. The IRPD spectrum of $H^+(CO_2)_2$-Ar, measured in the loss of Ar channel, is shown at the top of Figure 5. In comparison to the calculated spectrum, the photodissociation spectrum is much more complex with many additional features.

The most intense band located at 2400 cm^{-1} is assigned to the near degenerate in-phase/out-of-phase asymmetric CO_2 stretches. The center frequency of this band is at virtually the same position as the asymmetric CO_2 stretch of the $(OCOH)^+$-Ar complex, indicative of the negligible change in OCO bond lengths and angles upon formation of the dimer, in addition to the small perturbation of this motion due to the Ar. In the low-energy region of the spectrum, there are two nearly equally intense bands at 888 and 1026 cm^{-1}, which is the region predicted to include the $\nu_{sp}(\parallel)$ transition. Additionally, there are four bands, along with several weaker features, observed between 1345 and 1575 cm^{-1}. Given the mass selectivity of the experiment, it is not possible that any impurities are giving rise to these extra unexpected peaks. The multitude of bands must be due to the vibrational complexity inherent to the low C_1 symmetry $H^+(CO_2)_2Ar$ species. A summary of the experimental vibrational bands and corresponding assignments are presented in Table 1.

The bands centered at 888 and 1026 cm^{-1} are assigned to the out-of-plane $\nu_{sp}(\perp)$ and the $\nu_{sp}(\parallel)$ transitions, respectively. As shown in Figure 5, the harmonic frequency calculations predict $\nu_{sp}(\parallel)$ to be 10 times as intense as the out-of-plane $\nu_{sp}(\perp)$ transition. The relative intensities of the two experimental bands are suggestive of strong anharmonic coupling and intensity sharing between the two A symmetry vibrational motions involving the proton stretch. The two strong bands centered at 1345 and 1445 cm^{-1} fall in the region predicted to include the intense, in-plane $\nu_{sp}(\perp)$ transition (1385 cm^{-1}). While we have identified the calculated band as a shared proton stretch, this transition involves significant in-phase symmetric stretching and bending motion of the two CO_2 units involved in the proton bond. The CO_2 in-phase and out-of-phase symmetric stretch motions which do not involve proton motion are also predicted to fall in this spectral region, although they are expected to have much smaller oscillator strengths. Furthermore, there are four CO_2 bending vibrational modes predicted between 580 and 670 cm^{-1} for $H^+(CO_2)_2Ar$. It is therefore reasonable to conclude that the two experimental bands, along with other weaker structure in this region, may be associated with anharmonic coupling and intensity sharing between the in-plane $\nu_{sp}(\perp)$ mode and the CO_2 symmetric stretch motions and/or overtones of the CO_2 bends. Johnson and co-workers reported a similar intensity enhancement of intramolecular vibrations due to coupling to the shared proton vibrations in $(R_2O)_2H^+$, where R = Me, Et.[19]

As shown in Figure 5, there are also many weaker feature to the blue of the 1445 cm^{-1} band. Although assignments for these bands are more difficult to obtain, the inherent oscillator strengths of the shared proton motions may allow the observa-

tion of overtones at higher frequency. Along these lines, we assign the weaker features at 1575, 1695, and 2180 cm^{-1} to overtones of the out-of-plane $\nu_{sp}(\perp)$, $\nu_{sp}(\parallel)$, and in-plane $\nu_{sp}(\perp)$ modes, respectively. Turning our attention to the higher energy region of the spectrum, we find a 200 cm^{-1} broad feature centered at 3200 cm^{-1} and three weaker bands at 3570, 3715, and 3770 cm^{-1}. The latter are assigned to combination bands involving the in-plane $\nu_{sp}(\perp)$ mixed vibrations near 1350 cm^{-1} and the asymmetric CO_2 stretch vibrations at 2400 cm^{-1}. Similarly, the broad feature at 3200 cm^{-1} is attributed to the combination of the out-of-plane $\nu_{sp}(\perp)$ and $\nu_{sp}(\parallel)$ fundamentals with the asymmetric CO_2 stretch. The rich vibrational complexity in systems of this type should provide exacting tests for the highest levels of theory[13b, 16] aimed at predicting the extent to which the shared proton motions are coupled to the molecular cluster framework.

$H^+(CO_2)_3$−Ar. According to our calculations, the addition of a third CO_2 to the protonated dimer results in a structural rearrangement of the dimer core ion, leading to the "boat" structure shown in Figure 4c. This C_i boat structure is consistent with the global minimum $H^+(CO_2)_3$ structure determined previously by Gora et al.[39] A higher energy "chair" isomer (Figure 4e) was also determined previously,[38] and the higher level calculations reported here predict only a small 0.5 kcal/mol (170 cm^{-1}) energy difference between the two. Apparently, the third CO_2 stabilizes the boat structure in the trimer by making a three-centered, long-range electrostatic bond with the proton and the two partially positive carbon atoms. In comparison to the chair protonated CO_2 dimer, having an essentially linear OH^+O bonding motif, the boat trimer has an OH^+O bond angle of 171.2°, due to the interaction of the proton with the third, tethered CO_2.

The ab initio spectra are shown as smooth lines in Figure 6 for the boat (red) and chair (cyan) isomers of the protonated trimer. For the boat isomer there are now four characteristic shared proton vibrations spanning the 400 to 1200 cm^{-1} range of the spectrum, assigned to two $\nu_{sp}(\parallel)$ vibrations along with the in-plane and out-of-plane $\nu_{sp}(\perp)$ stretches. All of the assignments for the shared proton vibrations are summarized in Table 3. An interesting feature in the calculated spectrum is a 400 cm^{-1} separation between the two $\nu_{sp}(\parallel)$ vibrations, which is due to the difference in the accompanying intramolecular motions of the two core CO_2 molecules. For both the 400 and 800 cm^{-1} bands, the switchover of the proton between the lone pairs of the CO_2 molecules includes an out-of-phase CO_2 bending in the core. However, as the proton approaches the lone pair of one oxygen, the CO_2 unit is simultaneously bending that same oxygen either toward or away from the proton. The 400 cm^{-1} band corresponds to the latter scenario, which apparently results in a significant broadening of the proton-transfer potential and a correspondingly low frequency for the proton stretch.

The higher energy chair isomer consists of the protonated CO_2 dimer core ion with the third CO_2 interacting with the COH^+ region of one core CO_2. The result of this interaction is to localize the proton on the core CO_2 unit that interacts with the third, external CO_2, leading to OH^+ bond lengths of 1.090 and 1.334 Å. Once again the "solvent" induced asymmetry of the proton bond leads to a blue shift of $\nu_{sp}(\parallel)$ from the value of the analogous shared proton motion in the dimer. As shown in Figure 6 (cyan spectrum), the trimer chair isomer $\nu_{sp}(\parallel)$ is predicted to be near 1680 cm^{-1}, which should be compared to 770 cm^{-1} for the dimer.

Acquisition of the $H^+(CO_2)_3$ IRPD spectrum is again precluded due to the lack of a low-energy dissociation channel.

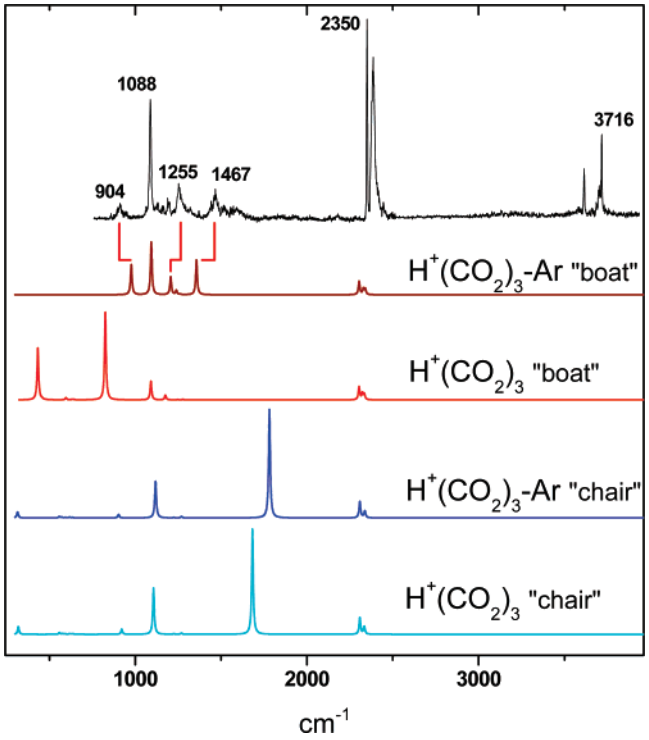

Figure 6. Comparison of the IRPD spectrum of $H^+(CO_2)_3Ar$ measured with the MP2 IR spectra of the two stable $H^+(CO_2)_3$ isomers, with and without Ar. All theoretical spectra are presented with correct relative IR intensities. The IR spectrum predicted for the "chair" isomer (blue) has an intense feature near 1780 cm^{-1} that is completely absent in the experimental spectrum. The bands observed between 700 and 1600 cm^{-1} agree well with the bands predicted by the harmonic frequency calculation for the "boat" $H^+(CO_2)_3Ar$ isomer (wine).

The MP2 binding energy of the third CO_2 to both isomers is ~3000 cm^{-1}, and the rare gas tagging method is required. Again, it is important to characterize the anticipated effect of the Ar on the band origins of the shared proton vibrations. For the higher symmetry boat isomer, the MP2 binding energy of Ar to the complex is 960 cm^{-1}. The calculated spectrum for the boat trimer−Ar complex is shown as the smooth wine-colored line in Figure 6. The two most intense features in the boat trimer spectrum (red) are now completely missing in the spectrum for the complex with Ar (wine). As observed for the protonated dimer, upon addition of Ar, the proton becomes less evenly shared with OH^+ bond lengths of 1.275 and 1.125 Å. Moreover, the Ar induced asymmetry results again in a blue shift of the two $\nu_{sp}(\parallel)$ vibrations. From the harmonic frequency calculations, the shared proton motion is fundamentally altered due to the asymmetry in the proton-transfer potential. The symmetries of the vibrations are largely reduced by the presence of Ar, and no vibrations in the complex correspond specifically to $\nu_{sp}(\parallel)$, which interchanges the proton between oxygen lone pairs. Instead, the modes (1206 and 1356 cm^{-1}) that are most like $\nu_{sp}(\parallel)$ in the bare boat trimer have motions that are more perpendicular to the OH^+O bond and involve a more substantial modification of the OH^+O bond angle. Regarding the in-plane and out-of-plane $\nu_{sp}(\perp)$ stretches, the Ar induced shifts are smaller and to the red (~70 cm^{-1}), consistent with the effect of Ar on the dimer $\nu_{sp}(\perp)$. The band positions of the calculated and experimental $H^+(CO_2)_3Ar$ species are summarized in Table 3, along with the assignments.

For the higher energy chair isomer, the MP2 binding energy of Ar to the complex is 790 cm^{-1}. The smooth blue curve in Figure 6 corresponds to the calculated spectrum for the chair trimer−Ar complex. As discussed above, the $\nu_{sp}(\parallel)$ vibration

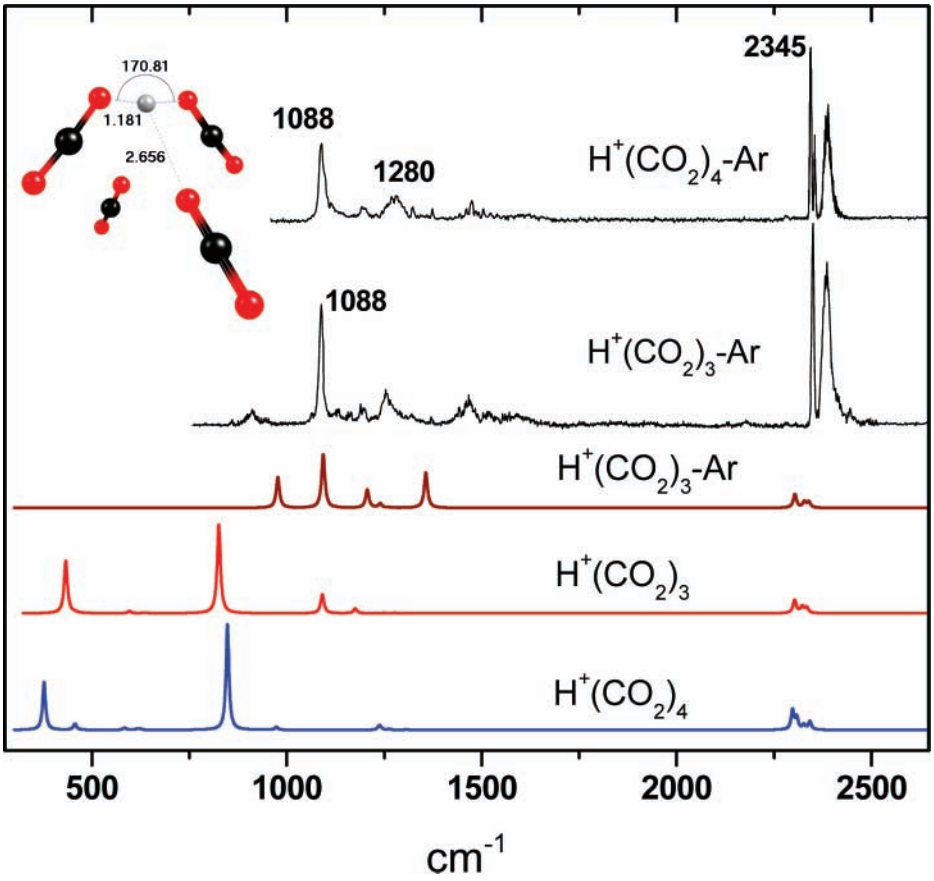

Figure 7. Comparison of the IRPD spectra of the $n = 3$ and $n = 4$ $H^+(CO_2)_n$ complexes measured in the Ar loss channel. The calculated spectra for $H^+(CO_2)_3$ and $H^+(CO_2)_4$ (both having the "boat" core dimer structure) both show $\nu_{sp}(\parallel)$ vibrations near 400 and 800 cm^{-1}. The two experimental spectra of the Ar-tagged complexes also have similar features, suggesting that the core dimer structure ("boat") and the effect of Ar upon the shared proton motion are similar for both cluster sizes. The MP2 structure of the $H^+(CO_2)_4$ complex is shown as an inset.

for this complex is predicted at 1680 cm^{-1}, and complexation with Ar leads to an additional 100 cm^{-1} blue shift. Along with the $\nu_{sp}(\parallel)$ blue shift, the addition of Ar to the chair trimer leads to a further reduction in the symmetry of the proton bond, with OH^+ bond lengths of 1.081 and 1.352 Å. Indeed, for the series of ions $H^+(CO_2)_2$, $H^+(CO_2)_2Ar$, chair $H^+(CO_2)_3$, and chair $H^+(CO_2)_3Ar$, the increasingly asymmetric sharing of the proton is accompanied by an incremental blue shift of the $\nu_{sp}(\parallel)$ vibration.

The IRPD spectrum of $H^+(CO_2)_3Ar$, measured in the loss of Ar channel, is shown at the top of Figure 6. The general qualitative features in the experimental spectrum agree quite well with the harmonic calculations for the Ar-tagged boat isomer. The intense band at 1780 cm^{-1} predicted for the chair isomer is completely missing, and we can therefore rule out the presence of this isomer in the experiment. This result is perhaps surprising given the relative energetics of the two isomers. Apparently, the exchange reactions present in the expansion are fast enough to allow the protonated trimer to rearrange to the global minimum boat structure. The bands centered at 904 and 1088 cm^{-1} are assigned to the out-of-plane and in-plane $\nu_{sp}(\perp)$ transitions, respectively. The broad bands centered near 1255 and 1470 cm^{-1} are then assigned to the two $\nu_{sp}(\parallel)$ vibrations. Once again, the broad structure in this region is at least partially due to the mixing of $\nu_{sp}(\parallel)$ with the intramolecular CO_2 symmetric stretches and bending overtones. The sharp, intense band at 1088 cm^{-1} suggests that the oscillator strength of the in-plane $\nu_{sp}(\perp)$ vibration is less diluted due to mixing with background levels, in comparison to the $\nu_{sp}(\parallel)$ vibrations. In the asymmetric CO_2 stretching region, there are now two bands; a sharp band is located at 2350 cm^{-1}, which is near the ν_3 transition for neutral CO_2, while a broader band is centered at 2385 cm^{-1}. The sharp band at 2350 cm^{-1} corresponds to the asymmetric CO_2 transition involving the linear "solvent" CO_2 in the boat trimer. The broader band is shaded to the blue and is composed of the unresolved in- and out-of-phase asymmetric CO_2 stretch motions of the core dimer. In comparison to the protonated dimer, this band is shifted by 15 cm^{-1} to lower energy. There are two additional sharp bands at 3614 and 3716 cm^{-1}, which are within 2 cm^{-1} of the well-known $(02^01)/(10^01)$ Fermi diad in neutral CO_2.[49] These bands are almost certainly due to a similar Fermi resonance involving the vibrations of the "solvent" CO_2 within the complex. As observed for the protonated dimer, there are also broad features in this region of the spectrum assigned to combinations of the shared proton motions with the asymmetric stretches of the core CO_2 units.

Larger Clusters. To further examine the structure of the protonated core dimer ion upon successive CO_2 solvation, we also measure the spectrum of the $H^+(CO_2)_4-Ar$ complex. A comparison of the $H^+(CO_2)_n-Ar$ ($n = 3, 4$) IRPD spectra are shown at the top of Figure 7. Except for the additional sharp band found in the asymmetric CO_2 stretch region, there is little difference in the two spectra, especially in the shared proton stretch region. The equilibrium structure of the protonated tetramer is shown as an inset in Figure 7, corresponding to a near C_{2v} structure with an equally shared proton between the two core CO_2 molecules in the boat configuration. The two relatively sharp CO_2 asymmetric stretch bands (2344 and 2355 cm^{-1}) are due to the in-phase and out-of-phase asymmetric

stretch motions of the "solvent" CO_2 molecules. A comparison of the predicted spectra for the $n = 3, 4$ complexes without Ar are shown at the bottom of Figure 7 (blue, red curves, respectively). Addition of the fourth CO_2 has little effect on the geometry of the core dimer, which leads to $\nu_{sp}(\parallel)$ band positions similar to those of the $n = 3$ complex. The binding energy of the fourth CO_2 molecule to the complex is ~2900 cm^{-1}, and once again, we cannot measure the IRPD spectra of the bare complex in the low-energy region of the spectrum. While we were unable to obtain converged structures and frequencies for the $H^+(CO_2)_4-Ar$ complex, the Ar induced asymmetry in the proton-transfer coordinate must be similar to the effect observed for the protonated trimer, given the close correspondence between the bands in the $\nu_{sp}(\perp,\parallel)$ region of the two IRPD spectra.

The rearrangement of the chair configuration found for the protonated CO_2 dimer to the boat structure upon addition of the third CO_2 is apparently preserved in the larger clusters. Successive solvation of the boat core ion has been examined up to $n = 7$ with MP2(fc) calculations and the smaller 6-31++g-(d,p) basis set, giving essentially the $n = 4$ structural motif with weakly attached CO_2 molecules occupying an effective second solvation shell. These results are in agreement with the previous theoretical study by Gora and co-workers, who examined the equilibrium structures up to $n = 6$.[39]

Conclusions

The infrared photodissociation (IRPD) spectra of $H^+(CO_2)_n-Ar$ are reported for $n = 1-4$ in the 700 to 4000 cm^{-1} region of the mid-IR. Both the ν_1 and ν_2 transitions are observed for the trans bent monomer structure, corresponding to the OH^+-Ar shared proton motion and the OCO asymmetric stretch, respectively. Interaction with the Ar ($D_e \sim 2400$ cm^{-1}) red shifts the ν_1 transition by 702 cm^{-1} from the OH^+ stretch transition in isolated $(OCOH)^+$. Progressions of the $(OCOH)^+Ar$ stretch are observed in combination with both the ν_1 and ν_2 transitions, which give an estimate of the intermolecular stretch frequency and the dissociation energy in the excited ν_1 and ν_2 states.

Ab initio calculations for the protonated CO_2 dimer predict a chair structure with the proton equally shared between the CO_2 oxygen lone pairs. Mass selection and IRPD of the $H^+(CO_2)_2-Ar$ complex reveals the shared proton stretch, $\nu_{sp}(\parallel)$, transition at 1026 cm^{-1}. The more evenly shared proton in the dimer, in comparison to the $H^+(CO_2)-Ar$ complex, leads to an approximately 1650 cm^{-1} red shift of the proton stretching frequency. The protonated dimer complex possesses rich vibrational complexity associated with the shared proton vibrations. The infrared spectrum in the shared proton region reveals resonances and intensity sharing between the bright, in-plane, $\nu_{sp}(\perp)$ transition and the dark background intramolecular vibrational levels.

Upon addition of a third CO_2, the IRPD spectrum, along with the ab initio calculations, reveal a structural rearrangement of the core dimer ion from the chair structure to a boat structure, with the axis of both CO_2 molecules positioned on the same side of the OH^+O axis. Successive solvation of the boat core dimer motif does not lead to any further rearrangement. For $n = 2$ to 4, ab initio calculations predict the addition of Ar leads to an uneven sharing of the proton, as observed previously for the protonated water dimer.[13] At the harmonic level, the reduced symmetry in the proton-transfer coordinate leads to significant blue shifts in the shared proton, $\nu_{sp}(\parallel)$ transitions. This effect is quite profound, in spite of the Ar binding perpendicular to the OH^+O axis, with an H^+-Ar bond distance of nearly 3.3 Å. Interestingly, these effects recovered with the harmonic approximation predict quite well the qualitative locations of the shared proton vibrations in the IRPD spectra. This is despite the anharmonicity certainly inherent in the shared proton motions.[13b] Infrared spectroscopic studies of other protonated molecular systems are currently underway to further investigate the structure and dynamics of the proton solvated in molecular clusters.

Acknowledgment. We gratefully acknowledge support for this work from the National Science Foundation (grant no. CHE-0551202).

Supporting Information Available: Full details of the ab initio computations done in support of the spectroscopy here, including the structures, energetics and vibrational frequencies for each of the isomeric structures considered. This information is available free of charge via the Internet at http://pubs.acs.org.

References and Notes

(1) Luecke, H.; Richter, H.-T.; Lanyi, J. K. *Science* **1998**, *280*, 1934−1937.
(2) Saraste, M. *Science* **1999**, *283*, 1488−1493.
(3) Wraight, C. A. *Biochim. Biophys. Acta* **2006**, *1757*, 886−912.
(4) Cleland, W. W.; Frey, P. A. *Science* **1994**, *264*, 1887−1890.
(5) Gerlt, J. A.; Kreevoy, M. M.; Cleland, W. W.; Frey, P. A. *Chem. Biol*. **1997**, *4*, 259−267.
(6) Tuckerman, M. E.; Marx, D.; Klein, M. L.; Parrinello, M. *Science* **1997**, *275*, 817−820.
(7) Marx, D. *Chem. Phys. Chem.* **2006**, *7*, 1848−1870.
(8) Voth, G. A. *Acc. Chem. Res.* **2006**, *39*, 143−150.
(9) Meot-Ner, M. *Chem. Rev.* **2005**, *105*, 213.
(10) Asmis, K. R.; Pivonka, N. L.; Santambrogio, G.; Brummer, M.; Kaposta, C.; Neumark, D. M.; Wöste, L. *Science* **2003**, *299*, 1375.
(11) Fridgen, T. D.; McMahon, T. B.; MacAleese, L.; Lemaire, J.; Maitre, P. *J. Phys. Chem. A* **2004**, *108*, 9008.
(12) (a) Headrick, J. M.; Diken, E. G.; Walters, R. S.; Hammer, N. I.; Christie, R. A.; Cui, J.; Myshakin, E. M.; Duncan M. A.; Johnson, M. A.; Jordan, K. D. *Science* **2005**, *308*, 1765. (b) Chang, H.-C.; Wu, C.-C.; Kuo, J.-L. *Int. Rev. Phys. Chem.* **2005**, *24*, 553−578.
(13) (a) Diken, E. G.; Headrick, J. M.; Roscioli, J. R.; Bopp, J. C.; Johnson, M. A. *J. Phys. Chem. A* **2005**, *109*, 1487. (b) Hammer, N. I.; Diken, E. G.; Roscioli, J. R.; Johnson, M. A.; Myshakin, E. M.; Jordan, K. D.; McCoy, A. B.; Huang, X.; Bowman, J. M.; Carter, S. *J. Chem. Phys.* **2005**, *122*, 244301.
(14) (a) Huang, X.; Braams, B. J.; Bowman, J. M. *J. Chem. Phys.* **2005**, *122*, 044308. (b) Kaledin, M.; Kaledin, A. L.; Bowman, J. M. *J. Phys. Chem. A* **2006**, *110*, 2933.
(15) (a) Kuo, J.-L. *J. Phys.: Conf. Ser.* **2006**, *28*, 87−90. (b) Shin, I.; Park, M.; Min, S. K.; Lee, E. C.; Suh, S. B.; Kim, K. S. *J. Chem. Phys.* **2006**, *125*, 234305. (c) Park, M.; Shin, I.; Singh, N. J.; Kim, K. S. *J. Phys. Chem. A.* **2007**, *111*, 10692. (d) Luo, Y.; Maeda, S.; Ohno, K. *J. Phys. Chem. A.* **2007**, *111*, 10732.
(16) Vendrell, O.; Gatti, F.; Meyer, H. D. *Angew. Chem., Int. Ed.* **2007**, *46*, 1−5.
(17) Moore, D. T.; Oomens, J.; Van Der Meer, L.; Von Helden, G.; Meijer, G.; Valle, J.; Marshall, A. G.; Eyler, J. R. *ChemPhysChem*. **2004**, *5*, 740.
(18) (a) Fridgen, T. D.; MacAleese, L.; Maitre, P.; McMahon, T. B.; Boissel, P.; Lemaire, J. *Phys. Chem. Chem. Phys.* **2005**, *7*, 2747. (b) Fridgen, T. D.; MacAleese, L.; McMahon, T. B.; Lemaire, J.; Maitre, P. *Phys. Chem. Chem. Phys.* **2006**, *8*, 955.
(19) Roscioli, J. R.; McCunn, L. R.; Johnson, M. A. *Science* **2007**, *316*, 249.
(20) (a) Yeh, L. I.; Okumura, M.; Myers, J. D.; Price, J. M.; Lee, Y. T. *J. Chem. Phys.* **1989**, *91*, 7319−7330. (b) Okumura, M.; Yeh, L. I.; Myers, J. D.; Lee, Y. T. *J. Phys. Chem.* **1990**, *94*, 3416.
(21) Ebata, T.; Fujii, A.; Mikami, N. *Int. Rev. Phys. Chem.* **1998**, *17*, 331.
(22) Bieske, E. J.; Dopfer, O. *Chem. Rev.* **2000**, *100*, 3963.
(23) Robertson, W. H.; Johnson, M. A. *Ann. Rev. Phys. Chem.* **2003**, *54*, 173.
(24) Duncan, M. A. *Intl. Rev. Phys. Chem.* **2003**, *22*, 407.
(25) Thaddeus, P.; Gueling, M.; Linke, R. A. *Astrophys. J.* **1981**, *246*, L41.
(26) Bogey, M.; Demuynck, C.; Destombes, J. L. *Astron. Astrophys.* **1984**, *138*, L41.

(27) Amano, T.; Tanaka, K., *J. Chem. Phys.* **1985**, *82*, 1045−1046.
(28) Amano, T.; Tanaka, K., *J. Chem. Phys.* **1985**, *83*, 3721.
(29) Bogey, M.; Demuynck, C.; Destombes, J. L. *J. Chem. Phys.* **1986**, *84*, 10.
(30) Bogey, M.; Demuynck, C.; Destombes, J. L.; Krupnov, A. *J. Mol. Struct.* **1988**, *190*, 465−474.
(31) Green, S.; Shor, H.; Siegbahn, P.; Thaddeus, P. *Chem. Phys.* **1976**, *17*, 479−485.
(32) Seeger, U.; Seeger, R.; Pople, J. A.; Schleyer, P. v. R. *Chem. Phys. Lett.* **1978**, *55*, 399−403.
(33) Frisch, M. J.; Schaefer, H. F., III; Binkley J. S. *J. Phys. Chem.* **1985**, *89*, 2192−2194.
(34) Yu, J. G.; Fu, X. Y.; Liu, R. Z.; Yamashita, K.; Koga, N.; Morokuma, K. *Chem. Phys. Lett.* **1986**, *125*, 438−442.
(35) Jacox, M. E.; Thompson, W. E. *J. Chem. Phys.* **2003**, *119*, 10824−10831.
(36) Dopfer, O.; Olkhov, R. V.; Roth, D.; Maier, J. P. *Chem. Phys. Lett.* **1998**, *296*, 585−591.
(37) Hiraoka, K.; Shoda, T.; Morise, K.; Yamabe, S.; Kawai, E.; Hirao, K. *J. Chem. Phys.* **1986**, *84*, 2091.
(38) Hiraoka, K.; Fujimaki, S.; Aruga, K. *Chem. Phys. Lett.* **1993**, *202*, 167−172.
(39) Szymczak, J. J.; Roszak, S.; Gora, R. W.; Leszczynski, J. *J. Chem. Phys.* **2003**, *119*, 6560−6570.
(40) Douberly, G. E.; Ricks, A. M.; Ticknor, B. W.; McKee, W. C.; Schleyer, P. v. R.; Duncan, M. A. *J. Phys. Chem. A* **2008**, *112*, in press.
(41) (a) Schmidt, M. W.; Baldridge, K. K.; Boatz, J. A.; Elbert, S. T.; Gordon, M. S.; Jensen, J. H.; Koseki, S.; Matsunaga, N.; Nguyen, K. A.; Su, S.; Windus, T. L.; Dupuis, M.; Montgomery, J. A. *J. Comput. Chem.* **1993**, *14*, 1347. (b) Gordon, M. S.; Schmidt, M. W. In *Theory and Applications of Computational Chemistry: The First Forty Years*; Dykstra, C. E.; Frenking, G.; Kim, K. S.; Scuseria, G. E., Eds.; Elsevier: Amsterdam, 2005; p 1167.
(42) Scott, A. P; Radom, L. *J. Phys. Chem.* **1996**, *100*, 16502−16513.
(43) Boys, S. F.; Bernardi, F. *Mol. Phys.* **1979**, *19*, 553.
(44) Illies, A. J.; Jarrold, M. F.; Bowers, M. T. *Int. J. Mass Spectrom. Ion Phys.* **1983**, *47*, 93−96.
(45) Shin, J.-W.; Hammer, N. I.; Diken, E. G.; Johnson, M. A.; Walters, R. S.; Jaeger, T. D.; Duncan, M. A.; Christie, R. A.; Jordon, K. D. *Science* **304**, 1137−1140.
(46) Francisco, J. S. *J. Chem. Phys.* **1997**, *107*, 9039−9045.
(47) Hammami, K.; Jaidane, N.; Lakhdar, Z. B.; Spielfiedel, A.; Feautrier, N. *J. Chem. Phys.* **2004**, *121*, 1325−1330.
(48) Hunter, E. P.; Lias, S. G., *NIST Chemistry WebBook*; NIST Standard Reference Database Number 69, National Institute of Standards and Technology: Gaithersburg, MD, (http://webbook.nist.gov), 2005.
(49) Chedin, A. *J. Mol. Spectrosc.* **1979**, *76*, 430.